JASA ARTICLE

The solution of sound propagation modeling problems for environment impact assessment by the mode parabolic equations method[a)]

Andrey G. Tyshchenko,[1] Mikhail A. Sorokin,[1] Sergey B. Kozitskiy,[1] and Pavel S. Petrov[2,b)]
[1]Geophysical Fluid Dynamics Laboratory, Il'ichev Pacific Oceanological Institute, Vladivostok 690041, Russia
[2]Instituto de Matemática Pura e Aplicada, Rio de Janeiro, CEP 22460-320, Brazil

ABSTRACT:
The method of sound propagation modeling based on the mode parabolic equations (MPEs) theory is applied to the verification scenarios for environmental impact assessment. The results for selected scenarios from the 2022 Cambridge Joint Industry Programme Acoustic Modelling Workshop and the configuration of the computational programs AMPLE and MPE for these scenarios is discussed. Furthermore, it is revealed how the results for these scenarios change in the case of the bottom slope across and along the propagation path. It is observed that for the cross-slope propagation scenario, the distribution of acoustic energy over decidecade frequency bands does not depend on the slope angle and is practically the same as that for range-independent environment. At the same time, the dependence of energy distribution is noticeable for up- and downslope propagation scenarios, where greater slope angles result in higher propagation loss. It is also shown that MPEs are capable of adequately handling typical sound propagation problems related to the environmental impact assessment for frequencies up to 1000 Hz. A possibility of using frequency-dependent mesh size and number of modes must be implemented in codes based on this approach.
 https://doi.org/10.1121/10.0034424

(Received 16 December 2023; revised 24 October 2024; accepted 29 October 2024; published online 15 November 2024)
[Editor: Martin Siderius] Pages: 3306–3319

I. INTRODUCTION

Mode parabolic equations (MPEs) theory has recently emerged as one of the promising tools for modeling of low-frequency sound propagation. Its development was originally motivated by executives of the Western Gray Whale program, which was undertaken jointly by the operators of Sakhalin-1 and Sakhalin-2 oil and gas projects on Sakhalin island (Russia; Rutenko *et al.*, 2015; Rutenko *et al.*, 2022). The primary aim of the program was the monitoring and preservation of the Okhotsk-Korean population of gray whales that spend summertime feeding on the benthos-rich Sakhalin shelf. Noise pollution caused, e.g., by seismic survey activities and supply vessel operation was identified as one of major factors of environmental impact within this program, and a clever thought was given to its assessment and mitigation.

One of the cornerstones of noise impact assessment are the tools for the modeling of sound propagation in three-dimensional (3D) shallow-water environments. To handle computational problems associated with such modeling, a technique based on the MPEs theory was developed (Petrov and Antoine, 2020; Petrov *et al.*, 2020; Trofimov *et al.*, 2015, 2018). Although the concept of MPEs originally was introduced by Collins (1993) and later generalized by Abawi *et al.* (1997), the development of our approach started with the papers by Trofimov (1999). His original results underwent major improvements in subsequent papers that prepared the basis for the computational program MPE based on the numerical solution of narrow-angle MPEs, where mode coupling was taken into account (Trofimov *et al.*, 2015, 2018). It is worth highlighting that the original derivation of MPEs within this approach is accomplished using the so-called method of multiple scales.

An alternative approach was proposed by Petrov and Antoine (2020), who used a somewhat more traditional derivation of MPEs involving a factorization of the operator in horizontal refraction equations (Jensen *et al.*, 2011). Such factorization results in a pseudo-differential mode parabolic equation (PDMPE) that can be very efficiently solved by the split-step Padé (SSP) method (Petrov and Antoine, 2020; Petrov *et al.*, 2020). PDMPEs have a very large aperture in the horizontal plane [some authors use the term extra-wide-angle parabolic equations (PEs) for such equations] and allow for very large steps in the marching variable, even exceeding the wavelength by a factor of 10. However, PDMPEs do not take mode interaction into account in their current implementation (the code called AMPLE), i.e., they are derived from adiabatic horizontal refraction equations, where the mode coupling terms are neglected (Jensen *et al.*, 2011).

[a)]This paper is part of a special issue on Verification and Validation of Source and Propagation Models for Underwater Sound.
[b)]Email: pavel.petrov@impa.br

It is important to stress that methods on which both AMPLE and MPE codes are based have been developed with 3D propagation problems in mind (which is very reasonable given the propagation conditions on the Sakhalin shelf). Thus, in the verification scenarios A1 and B1 from the 2022 Joint Industry Programme (JIP) Acoustic Modelling (JAM) Workshop (Ainslie *et al.*, 2024) discussed in the present work, both models cannot fully reveal their strengths. On the contrary, they simply require excessive computational effort in two-dimensional (2D) range-independent propagation scenarios, where mode amplitudes can be computed analytically. We, therefore, modified the broadband range-independent scenario B1 by making the seabottom sloping and studied the dependence of modeling results on the slope angle for the cases when propagation path is aligned along or across the depth gradient.

We also find it important to provide potential users of our models with a detailed explanation of how such cases should be handled in practice. This includes the choices of computational grids for PE, the number of normal modes that should be taken into account, bottom truncation depth, and other parameters that are usually not discussed in the papers where the capabilities of MPEs to take 3D effects into account are highlighted. Our aim here is to provide interested users with a tutorial on configuration of the MPE-based models that can be subsequently used for solving more complex problems (as the parameters mentioned above would not drastically change in the case of an environment with, e.g., more complicated 3D bathymetry features and a nontrivial sound speed distribution).

The article is organized as follows. First, we briefly introduce both computational models involved (Sec. II). Second, we study the JAM workshop scenarios A1 (Sec. III) and B1 (Sec. IV). Next, we also investigate the modified B1 scenario with the bottom slope across (Sec. V) and along (Sec. VI) the sound propagation path (i.e., the source-receiver line). Finally, the key findings are summarized in the conclusion (Sec. VII).

Throughout this study, we maintain consistency with the notation from Ainslie *et al.* (2022) and the related ISO 18405 terminology standard (ISO, 2017).

II. MPES THEORY

Within the MPEs theory (Abawi *et al.*, 1997; Collins, 1993; Petrov *et al.*, 2020; Trofimov, 1999), acoustic field in a 3D range-dependent waveguide is presented in the form of an expansion over normal modes (Jensen *et al.*, 2011; Katsnelson *et al.*, 2012) such that

$$P(f,x,y,z) = S(f)\sum_{m=1}^{M} A_m(x,y)\phi_m(z,x,y), \qquad (1)$$

where $S(f)$ is the source spectrum, $\phi_m(z,x,y)$ are eigenfunctions of the modes (in principle, for any fixed pair x,y, they are functions of the depth z; however, in the range-dependent environment, they also parametrically depend on the horizontal coordinates), and $A_m(x,y)$ are the respective mode amplitudes. In simple words, A_m are coefficients of the field representation in the basis $\{\phi_m\}$, whereas the basis itself varies on the horizontal coordinates x, y.

In the simplest case of the range-independent environment, the basis is the same in the entire computational domain (i.e., for all x, y), whereas the mode amplitudes can be computed by a simple analytical formula, and Eq. (1) can be rewritten as

$$P(f,x,y,z) = \frac{\mathrm{i}}{4\rho_w} S(f)\sum_{m=1}^{M} H_0^{(1)}(k_m r)\phi_m(z_s)\phi_m(z), \qquad (2)$$

where z_s is the source depth (it is deployed at $x=0, y=0, z=z_s$), r is the range, $r=\sqrt{x^2+y^2}$, and k_m is the horizontal wavenumber of the mth mode.

Note that the main issues associated with the implementation of Eq. (2) are the truncation of the computational domain in z and truncation of the infinite series over the modes at $z=H$. There are ways to handle the infinite bottom halfspace, but they require computations of branch line integrals that render the correct computations in the range-dependent scenarios impractical. In the models described below, the total depth of the computational domain is always finite, i.e., we solve the problem for $z \in [0,H]$, where H is sufficiently large. In addition to MPE-based models that are designed to handle 3D inhomogeneous media, we also use a simple code for 2D range-independent scenarios, called ac_modes (available online[1]), written in MATLAB (MathWorks, Natick, MA) and validated via comparisons with well-known Kraken and Orca solvers as well as the source images solution (Deane and Buckingham, 1993) for the special case of the horizontal bottom (we use discretization of $\Delta z = 0.125$ m in depth and the same truncation depth and mode numbers as were used for AMPLE).

A. AMPLE: A code based on PDMPEs

The first model that was used in this study is called AMPLE (ample-angle mode parabolic equation; see Petrov and Tyshchenko, 2020; Petrov *et al.*, 2020; Tyshchenko *et al.*, 2021). Within the latest stable version of the AMPLE code based on PDMPEs, mode amplitudes $A_m(x,y)$ in Eq. (1) are computed in adiabatic approximation by solving one-way counterpart of the horizontal refraction equations

$$\frac{\partial^2 A_m}{\partial x^2} + \frac{\partial^2 A_m}{\partial y^2} + k_m^2(x,y)A_m = -\phi_m(z_s)\,\delta(x)\delta(y), \quad m = 1,\ldots,M. \qquad (3)$$

Introducing a reference horizontal wavenumber, e.g., the one in the vicinity of the source, $k_{m,0} = k_m(0,0)$, we cancel out the principal oscillation in A_m such that

$$A_m(x,y) = \mathrm{e}^{\mathrm{i}k_{m,0}x} B_m(x,y),$$

and hereafter solve an equation for the envelope function $B_m(x,y)$.

Obtaining a one-way counterpart of an equation for B_m and formally integrating it with respect to x on a small interval $\Delta x = h$, we obtain the propagator $\hat{P}$, which has the form

$$B_m^{n+1} = \exp\left(\mathrm{i}k_{j,0}h\left(\sqrt{1+\hat{L}_m}-1\right)\right)B_m^n \equiv \hat{P}B_m^n, \tag{4}$$

where by definition $B_m^n(y) = B_m(x_n, y)$ (assume that a uniform grid in x is introduced, $x_{n+1} - x_n = h$), and $\hat{L}_m = (\partial_y^2 + k_m^2 - k_{m,0}^2)/k_{m,0}^2$. A marching scheme that computes the propagators [Eq. (4)] can be designed using the SSP method (Petrov *et al.*, 2020) with suitable perfectly matched layers (PML) or transparent boundary conditions (TBCs) and a wide-angle starter for modeling a point source.

The program AMPLE has been in development since 2019 in C++ programming language. It is based on the computation of acoustic field by Eq. (1), where the mode amplitudes are computed by solving the respective PDMPEs by the SSP method. The program implements the computation of 3D acoustic pressure, particle acceleration, and sound exposure level (SEL) fields, as well as the calculation of modal functions and their respective wavenumbers. AMPLE is also capable of computing sound pulse waveform (i.e., the sound pressure as a function of time) at specified receiver locations. The outputs are computed for a user-defined area specified by a uniform computational grid. The input data includes information on the bottom layers' structure (sound speed, density, and attenuation), hydrology (sound speed distribution inside the water column), and bathymetry. 3D distributions of acoustic pressure, particle acceleration, and SEL are output on the same grid. For mode computation, AMPLE uses the normal modes toolbox CAMBALA (Petrov *et al.*, 2019). AMPLE receives input data as a configuration file in JSON format that specifies media parameters and mode computation parameters, frequencies, source function or spectrum, precomputed modal functions and wavenumbers (if necessary), receiver points, and PE parameters (Padé approximation order, initial and boundary conditions, etc.). The dimensions of multidimensional input and output data are specified in JSON format and the data itself can be stored in either text or binary files in row-major order. The program employs a command line interface, allowing the user to specify what should be computed, how the results should be output, and how many processes to use for computation. The source code and sample configurations are available on GitHub (Petrov and Tyshchenko, 2020).

B. Narrow-angle MPEs with modes interaction

The program MPE is based on the theory of narrow-angle MPEs with mode interaction that was developed in Trofimov *et al.* (2015, 2018). For the reader's convenience, we reproduce the main equations of this theory here.

Let us represent the bathymetry in the domain of interest by the function $h(x,y)$,

$$h(x,y) = h_0(x) + h_1(x,y), \tag{5}$$

where h_1 is considered to be a small transverse variation of the profile h_0 along the preferred direction of propagation. The sound speed distribution is also recast in the form

$$\frac{\omega^2}{c^2} = \kappa^2(x,z) + \nu(x,y,z), \tag{6}$$

where ν is small in comparison to κ^2.

In these notations, narrow-angle MPE with mode interaction can be written as

$$2\mathrm{i}\mathbf{K}\mathbf{b}_x + \mathrm{i}\mathbf{K}'\mathbf{b} + \mathbf{b}_{yy} + \boldsymbol{\Xi}\mathbf{b} = 0, \tag{7}$$

where $\mathbf{K} = \mathbf{K}(x) = \mathrm{diag}(k_1(x,0), k_2(x,0), \ldots, k_M(x,0))$ is a diagonal matrix formed by the horizontal wavenumbers computed at $y=0$, and vector function $\mathbf{b}(x,y)$ represents the envelope function for mode amplitudes

$$\mathbf{a}(x,y) = \mathrm{e}^{\mathrm{i}\boldsymbol{\Phi}(x)}\mathbf{b}(x,y),$$

and the mode interaction matrix $\boldsymbol{\Xi}(\mathbf{x},\mathbf{y})$ has the form

$$\boldsymbol{\Xi}(x,y) = \mathrm{e}^{-\mathrm{i}\boldsymbol{\Phi}(x)}\mathbf{T}(x,y)\mathrm{e}^{\mathrm{i}\boldsymbol{\Phi}(x)},$$
$$\boldsymbol{\Xi}_{nm}(x,y) = \mathbf{T}_{nm}(x,y)\mathrm{e}^{\Phi_n(x)-\Phi_m(x)}.$$

The elements of the matrix $\mathbf{T}$ are defined by the formula

$$\begin{aligned}\mathbf{T}_{nm}(x,y) = {} & \int_0^H \frac{1}{\rho}\nu\phi_m\phi_n\,dz - \mathrm{i}k_m(V_{nm}-V_{mn}) \\ & + \Bigg\{ h_1\phi_m\phi_n\left[k_m^2\left(\frac{1}{\rho_+}-\frac{1}{\rho_-}\right) - \left(\frac{\omega^2}{c^2\rho}\right)_+ \right. \\ & \left. + \left(\frac{\omega^2}{c^2\rho}\right)_-\right] - h_1\frac{1}{\rho^2}\phi_{m,z}\phi_{n,z} \\ & \times \left[(\rho)_+ - (\rho)_-\right]\Bigg\}\Bigg|_{z=h_0},\end{aligned}$$

where the term in the braces is computed in a more general case for all media interfaces, and $V_{mn} = \int_0^H (1/\rho)\phi_{m,x}\phi_n\,dz$. Note that MPEs in Eq. (7) are formally derived by the method of multiple scales (it can be also considered as a generalization of Wentzel-Kramers-Brillouin-Jeffreys to the case of vector functions as shown in Trofimov *et al.*, 2023). For this reason, the requirements in Eqs. (5) and (6) are also somewhat formal.

From the expressions for coupling terms $\mathbf{T}_{nm}(x,y)$, one can conclude that the MPEs in Eq. (7) do not preserve energy flux unlike some other models based on normal modes theory (mostly available for 2D problems; e.g., Abawi, 2002; Godin, 1998; Tromp, 1994). However, as the MPE approximation is of asymptotic nature, it is natural to expect asymptotic energy flux conservation (modulo some higher-order terms with respect to the small parameter). This property was established in Trofimov *et al.* (2015) in the form of a theorem.

TABLE I. Media parameters are shown for the case A1, with a 50 m water layer overlying a fluid sediment halfspace.

Layer	Thickness (m)	Density (kg/m^3)	Sound speed (m/s)	Attenuation (dB/λ)
Water	50	1	1500	0
Sediment	∞	2	1700	0.5

Based on the narrow-angle MPE theory, the program MPE has been in development from 1997 to 2023. It consists of five modules that provide numerical simulations of various acoustic 2D and 3D sound propagation problems using different mathematical methods. The first module is a toolbox for reading and preprocessing the input data required for further computations. The data consist of bathymetry and bottom layers' specifications (depth, density, and sound speed). The second module calculates modal functions and their respective wavenumbers using the inverse iteration and bisection methods, respectively. The values are computed along the path (or paths) of sound propagation, and Richardson's extrapolation technique of arbitrary order can be applied to improve the accuracy of the eigenvalue problem solution. The third module provides numerical solutions to MPEs with or without mode interaction in 2D scenarios, whereas the fourth module handles sound propagation in 3D layered media. The latter implements adiabatic and coupled modes narrow-angle MPE solution (Trofimov *et al.*, 2015) by the Crank-Nicolson method with the Gaussian starter (Jensen *et al.*, 2011) and PML for artificial domain truncation. The module outputs acoustic pressure field as well as particle velocities, and accelerations are obtained. The fifth module is used to simulate the propagation of sound pulses by the Fourier synthesis method. It can be applied for the 2D and 3D scenarios in adiabatic or interacting modes propagation regimes. It allows to compute acoustic pressure waveforms as well as the respective components of particle acceleration at arbitrarily placed receivers (the number of which is not limited). At the same time, power spectra of acoustic pressure and particle acceleration for each of the receivers are also obtained. The program MPE is developed in the C++ language with the graphic user interface implemented with Microsoft Foundation Class Library. The output consists of several MATLAB (MathWorks, Natick, MA) matrices, CSV, and plain text files, where each contain one of the computed tensors: sound pressure, sound pulse waveforms, particle accelerations, and velocities.

III. CASE A1

In this section, we consider a shallow-water range-independent waveguide up to the range of 30 km. The monopole point source is located at $x = 0, z_s = 5$ m. Media parameters provided in the workshop specification (Ainslie *et al.*, 2024) are shown in Table I (the same scenario was used at the previous JIP workshop; see Ainslie *et al.*, 2019a; Ainslie *et al.*, 2019b). The acoustic source emits a sine waveform at a fixed frequency. Sound propagation modeling was performed using AMPLE and MPE, as well as ac_modes, which actually uses range-independent formula Eq. (2). We performed computations only for frequencies up to 1 kHz as all our codes were designed to handle low-frequency propagation scenarios (using normal modes is hardly an optimal solution for $f > 1$ kHz).

Because AMPLE and MPE operate in 3D environments, the actual computation area is extended to $0 \leqslant x \leqslant 30\,000, -1500 \leqslant y \leqslant 1500$. To avoid dealing with branch line integrals, we also truncated the computational domain in z at $z = H$ (the quantity H can be frequency dependent, and a rule of thumb can be $H \sim 30\lambda$, i.e., few tens of wavelengths). The grid parameters also depend on the source frequency as shown in Table II. Note that we present the largest possible values of Δx and Δy for which the solution still converges, although we computed the propagation loss (PL) curves in the figures below with higher resolution to make them look smoother. Ideally, the grid resolution Δy in the transverse direction for both models is chosen from the requirement that there are no less than 5 points per horizontal wavelength (although we reduce this number to 3 points per horizontal wavelength at 1 kHz). For MPE, the step in range, Δx, must be comparable to Δy, whereas for AMPLE, it can be much larger than the wavelength resulting from the capabilities of SSP integration technique.

For AMPLE and MPE programs, the modes were computed with the mesh size $\Delta z = 0.1$ m (this is more than enough to accurately resolve vertical modes at all frequencies involved), although higher accuracy would not pose any difficulties as even in the range-dependent scenarios, the computation of normal modes for the entire domain takes an insignificant portion of total computational time (especially if certain mathematical tricks are used to improve its efficiency). Configuration files for AMPLE program can be found at the respective GitHub repository (Petrov and Tyshchenko, 2020).

TABLE II. The configuration parameters are displayed for the programs AMPLE and MPE in scenario A1 (including grid parameters in the horizontal plane and truncation depth $z = H$ for which the modes were calculated), and the total computational time for each frequency.

	AMPLE			MPE				
Frequency (Hz)	Δx (m)	Δy (m)	Time (s)	Δx (m)	Δy (m)	Time (s)	H (m)	Number of modes
10	450	2	8	10	6	120	4800	50
50	100	1	12	5	2	180	2500	2
100	50	0.5	15	4	1	300	1500	3
1000	5	0.5	1200	1	0.5	12 600	1000	32

According to the description of verification scenarios, the output of the following quantities was requested (Ainslie *et al.*, 2024):

$$N_{\mathrm{PL},p}(x,y,z) = -20\,\log_{10}\left|\frac{p(x,y,z)}{p_0}\right|, \tag{8}$$

$$N_{\mathrm{PL},a}(x,y,z) = -20\,\log_{10}(a(x,y,z)), \tag{9}$$

where

$$a(x,y,z) = \sqrt{|a_x|^2 + |a_y|^2 + |a_z|^2} \tag{10}$$

is the magnitude of the particle acceleration.

The values of $N_{\mathrm{PL},p}$ and $N_{\mathrm{PL},a}$ are output at $y=0$ and $0 \leqslant x \leqslant 30\,000$ at receiver depth $z_r = 15\,\mathrm{m}$ (see Figs. 1 and 2). Additionally, $N_{\mathrm{PL},p}$ and $N_{\mathrm{PL},a}$ are output at $y=0, x = 12\,500$ and $0 \leqslant z \leqslant 50$ (see Fig. 3). Because the waveguide parameters are range independent, we have $a_y|_{y=0} \equiv 0$ (and $a_x = a_r$). Reference solutions are obtained by `ac_modes` and (in some cases) the widely used Gaussian beam-based tool `BELLHOP`. Apart from some discrepancies with `BELLHOP` in the near field, all of the solutions agree very well.

As with many PE-based computational tools, it is important to properly set up the grids for `AMPLE` and `MPE` as well as to choose the number of modes M taken into account. Following is the explanation of how these parameters should be chosen.

`AMPLE` and `MPE` programs allow one to specify the number of modes M directly and restrict oneself to waterborne (guided) modes only. In `AMPLE`, there is also a possibility to take all modes with grazing angles within certain interval into account. In this scenario, we perform computations with waterborne modes for $f \geq 50\,\mathrm{Hz}$ (exact numbers are given in Table II) while setting $M = 50$ for $f = 10\,\mathrm{Hz}$ (as there are no waterborne modes). This explains the discrepancy with `BELLHOP` in the near field where higher-order modes also contribute to the total field, although for $x > 200\,\mathrm{m}$, their contribution becomes negligible as observed in Fig. 1. Clearly, it is not difficult to eliminate this discrepancy by taking more modes into account. This would lead to a proportional increase in the computational time and, therefore, the decision on this matter should depend on the user's priorities.

The domain truncation depth H should be large enough to properly handle attenuation effects in the near field. For `AMPLE` and `MPE`, a good balance between performance and accuracy is

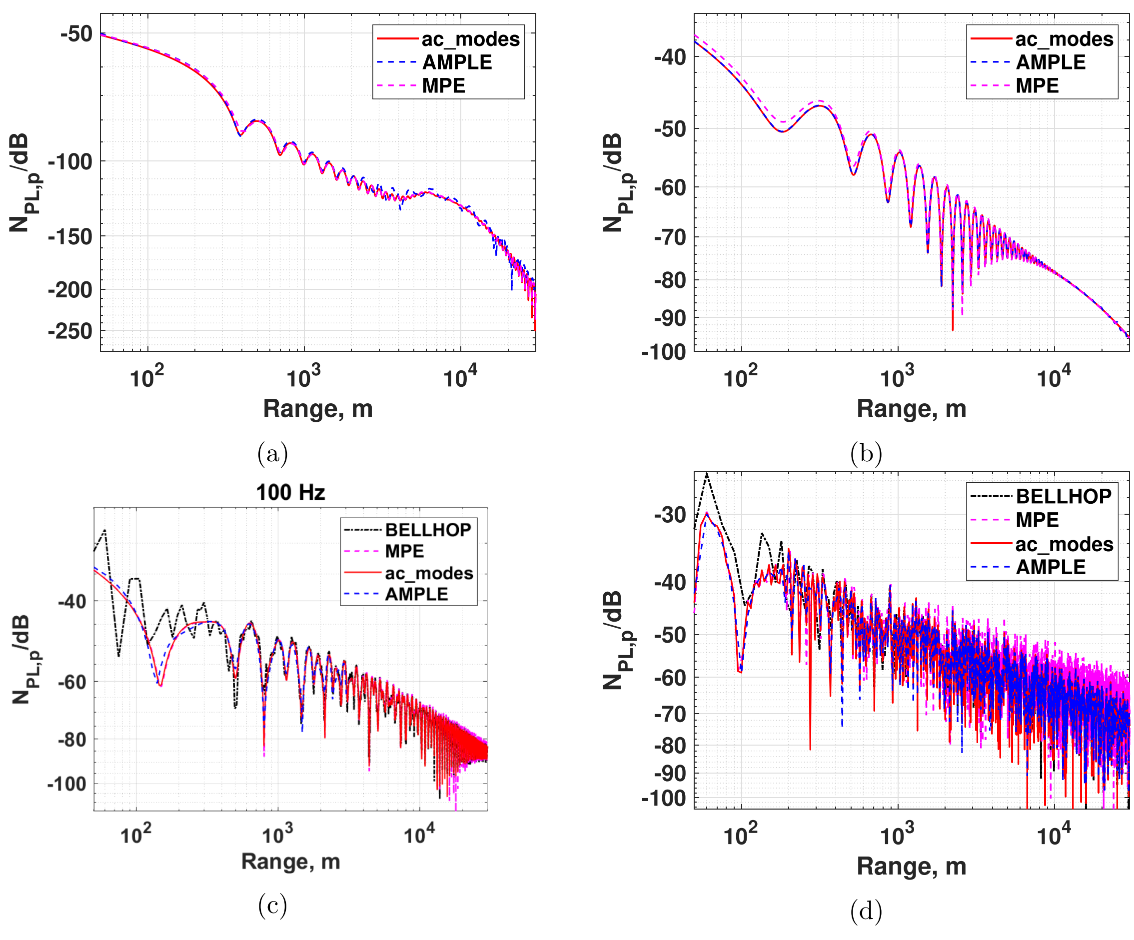

FIG. 1. (Color online) $N_{\mathrm{PL},p}(x,0,z_r)$ are displayed for the frequencies 10 Hz (a), 50 Hz (b), 100 Hz (c), and 1000 Hz (d) as a function of range at the fixed depth $z = z_r = 15\,\mathrm{m}$, computed using `AMPLE` (dashed blue line), `MPE` (dashed magenta), and reference solutions computed using `BELLHOP` (dashed-dotted black) and `ac_modes` (solid red).

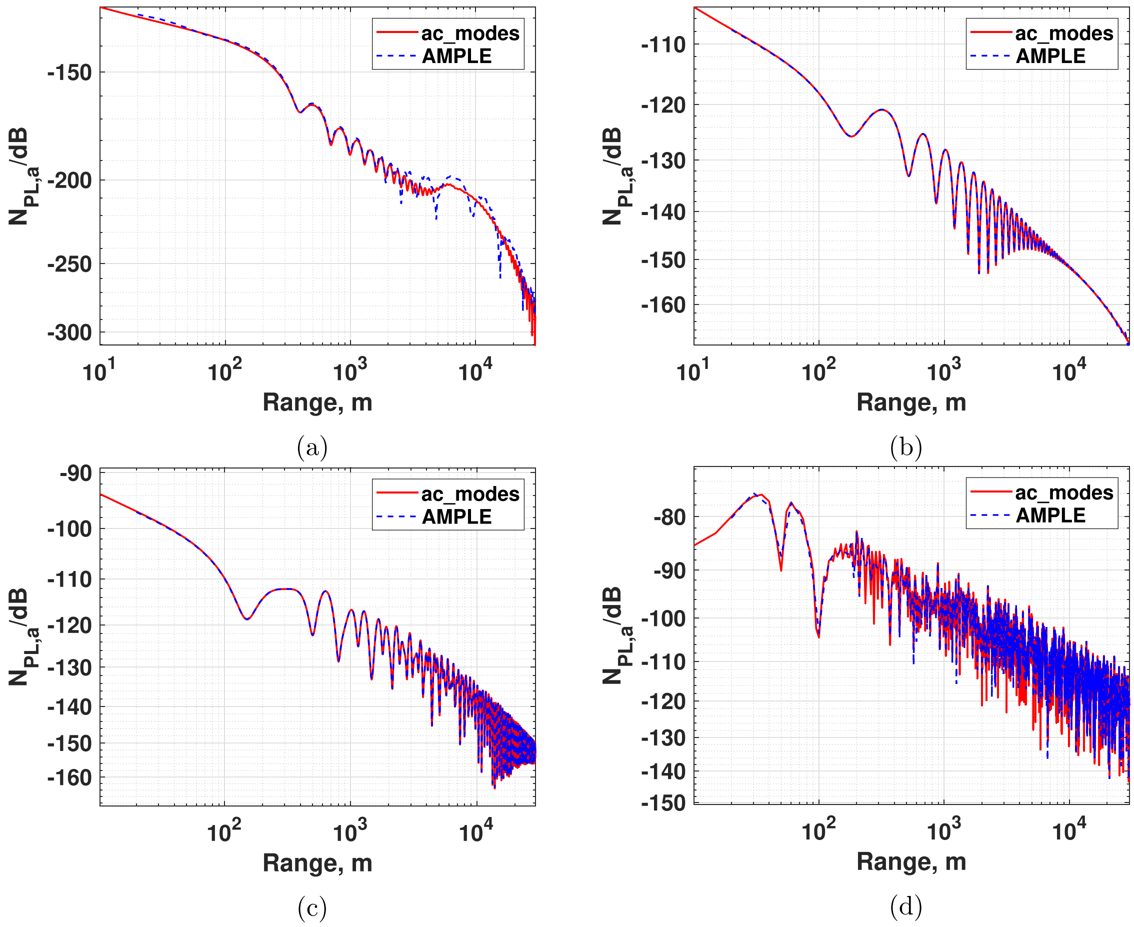

FIG. 2. (Color online) Particle acceleration $N_{\mathrm{PL},a}(x,0,z_r)$ are displayed for the frequencies 10 Hz (a), 50 Hz (b), 100 Hz (c), and 1000 Hz (d) as a function of range at the fixed depth $z = z_r = 15$ m.

$$H(\lambda) = 30\lambda,$$

where $\lambda = c/f$ is the wavelength (this is a heuristic formula obtained by running convergence tests; however, if necessary, the value can be decreased by adding an absorbing layer near the truncation depth).

For MPE and AMPLE, it is also important to choose the appropriate step size over the x and y coordinates for the solution to converge. In general, the step size can be chosen for AMPLE as

$$\begin{aligned} &dx < 3\lambda, \\ &dy = 0.5, \quad \lambda \le 15\,\mathrm{m}, \\ &dy = 1, \quad \lambda \ge 15\,\mathrm{m}, \end{aligned} \tag{11}$$

and for MPE as

$$dx = 0.2\lambda, \quad dy = \frac{dx}{2}. \tag{12}$$

The possibility of using large steps in range in AMPLE is a feature of the SSP method used for the PDMPE integration.

The initial conditions employed by MPE and AMPLE also differ. As MPE is based on the narrow-angle PE, it uses the Gaussian starter that provides an appropriate aperture for this case. On the other hand, AMPLE requires the initial condition to have sufficient aperture to handle wide-angle propagation. For this reason, AMPLE uses a simplified version of the ray starter (Petrov *et al.*, 2020), based on the ray theory in the near field. This starter provides an arbitrary aperture in the horizontal plane.

In low-frequency cases, AMPLE typically produces the solution in a few tens of seconds (see Table II), whereas for MPE, it takes a few minutes to handle such cases (partly due to smaller steps in range, and partly because it spends additional effort to take mode interaction into account). Both models become substantially less efficient for frequencies above 500–600 Hz, e.g., it takes 20 min and ca. 4 h to solve the 1 kHz case with AMPLE and MPE, respectively.

Note that the computation of particle acceleration within this approach requires no additional computational effort, and both programs maintain the same accuracy as for acoustic pressure when calculating this quantity.

IV. CASE B1

The environment in scenario B1 is the same as that in Sec. III. However, the goal is to perform the simulation of a broadband signal emitted by a monopole source. The source waveform (single airgun) depicted in Fig. 4 was provided by

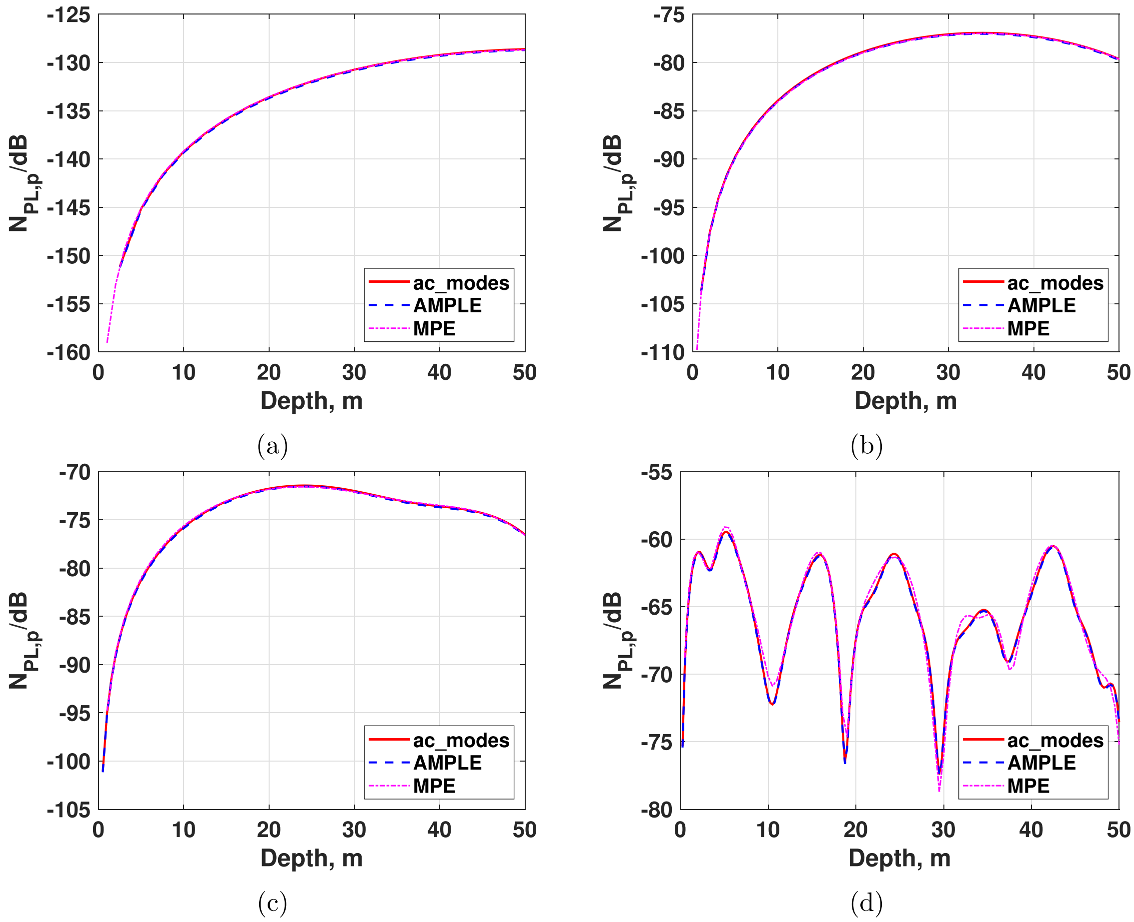

FIG. 3. (Color online) Acoustic pressure $N_{PL,p}(x = 12.5\,\text{km}, z)$ are displayed for the frequencies 10 Hz (a), 50 Hz (b), 100 Hz (c), and 1000 Hz (d) as a function of *depth* at the fixed range $x = 12.5$ km.

the workshop organizers (Ainslie *et al.*, 2024). The source position is the same as that in case A1, and receivers are located at points $\mathbf{r}_1 = (30\,\text{m}, 0, 15\,\text{m})$ and $\mathbf{r}_2 = (3000\,\text{m}, 0, 15\,\text{m})$ (Fig. 5).

The quantities to be computed in this scenario are sound pulse waveform, $p(t)$, at both receivers and their respective spectra, $P(f)$. The spectra of the particle acceleration components $|A_r(f)|$, $|A_z(f)|$ along r and z axes were also required. By the definition,

$$P(f) = \int_{-\infty}^{\infty} p(t) \exp(2\pi i f t) dt, \tag{13}$$

$$\mathbf{A}(f) = \int_{-\infty}^{\infty} \mathbf{a}(t) \exp(2\pi i f t) dt, \tag{14}$$

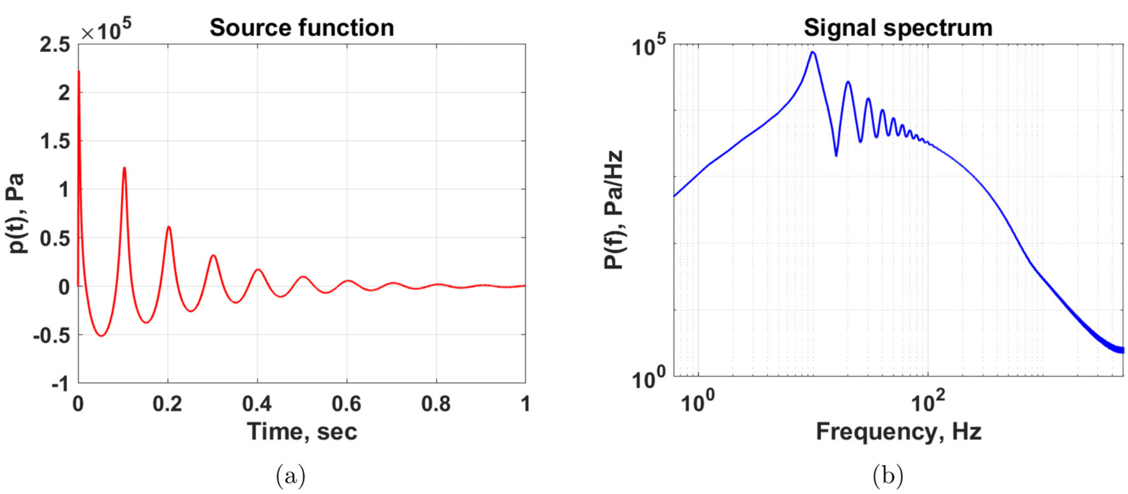

FIG. 4. (Color online) Source function and its spectrum.

https://doi.org/10.1121/10.0034424

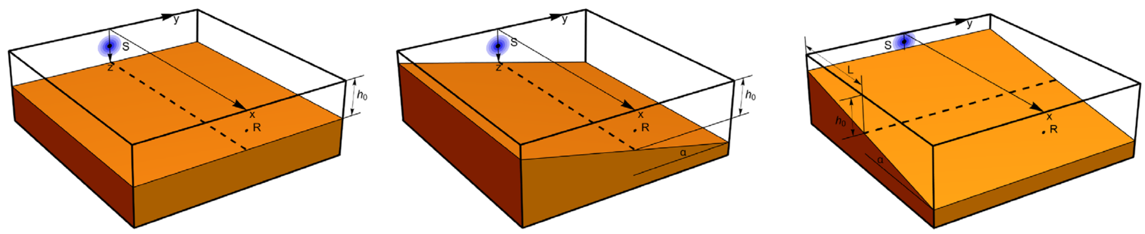

(a) (b) (c)

FIG. 5. (Color online) Environment in the B1 scenario (a) (Sec. IV) and its generalizations, where across-slope propagation (b) (Sec. V) and downslope propagation (c) (Sec. VI) are considered. In all cases, the source is located at $x = 0$, $y = 0$, $z = z_s = 5\,\mathrm{m}$. The receiver is located at $x = 3\,\mathrm{km}$, $y = 0$, $z = z_r = 15\,\mathrm{m}$.

where $\mathbf{a}(t)$ and $\mathbf{A}(f)$ are vectors formed by r and z coordinates of the particle acceleration in the time and frequency domains, respectively, such that

$$\mathbf{a}(t) = (a_r(t), a_z(t)), \tag{15}$$

$$\mathbf{A}(f) = (A_r(f), A_z(f)). \tag{16}$$

The computations for scenario B1 were also performed using AMPLE, MPE, and ac_modes. The computational grid and mode parameters for MPE and AMPLE are shown in Table III, and full configuration files for AMPLE are available at GitHub (Petrov and Tyshchenko, 2020).

All computations were performed with the frequency range from 1 to 1000 Hz. Truncation depth and dz for ac_modes vary with frequency for better efficiency of a relatively slow MATLAB code.

In this case, it turned out that MPE outperforms AMPLE as the former allows to adjust mesh size according to frequency by Eq. (12). The computations with AMPLE were performed using the same grid for all frequencies, i.e., the steps were chosen in such a way that they fulfill the condition (11) for the highest frequency $f = 1000\,\mathrm{Hz}$. As a result, the computations with AMPLE took approximately twice as much time as those with MPE, e.g., 14 and 5 h, respectively, for the receiver at $x = 3\,\mathrm{km}$) for a single-thread computation on a personal computer (PC) with an Intel Core i9-13900KF central processing unit (CPU; Intel, Santa Clara, CA) and 256 Gb random access memory (RAM). However, AMPLE on the same PC can solve the same problem in less than 1 h by using multiple computational threads (28 threads).

In this scenario, the receiver at $x = 30\,\mathrm{m}$ is located in the near field of the source. Thus, not only waterborne modes must be taken into account at this point. We accounted for all modes with the grazing angle of less than 30° for all frequencies when performing computations using AMPLE. In the case of MPE, we took into account the first 200 modes for each frequency (unless there were fewer than 200 propagating modes).

TABLE III. Configuration for MPE and AMPLE programs in case B1.

	AMPLE		MPE	
Program	$x = 30\,\mathrm{m}$	$x = 3\,\mathrm{km}$	$x = 30\,\mathrm{m}$	$x = 3\,\mathrm{km}$
M	$\operatorname{acos}\frac{k_j}{k_w} < \frac{\pi}{6}$	32	200	100
Time (min)	30	840	15	310
H (m)	2750		600	

The comparisons of the results obtained with the different methods are displayed in Figs. 6 and 7. The results for particle accelerations in Fig. 7 are presented only in the frequency domain. Perfect agreement is also achieved in the time domain, although the waveforms are quite similar to the waveform of acoustic pressure in Fig. 6 and we do not present them here.

V. PROPAGATION PARALLEL TO THE APEX OF THE WEDGE

In this section, we consider a modified version of the broadband propagation scenario from Sec. IV. Our goal is to investigate how accurately AMPLE and MPE reproduce the field for different angles of bottom slope in the direction across the propagation path. In fact, this is a short-range broadband generalization of the well-known wedge benchmark scenario (Jensen *et al.*, 2011; Petrov *et al.*, 2020; Petrov and Sturm, 2016). In the previous work on validation of both models used in this study, the wedge problem was successfully solved for single frequencies (e.g., 25 Hz in the well-known wedge benchmark; Jensen *et al.*, 2011). However, it is the first time that we investigate the accuracy of MPE solutions for a relatively broad frequency range from 10 Hz to 1 kHz. To restrict the number of figures in this section (as well as in Sec. VI, where downslope propagation is considered), we study only the spectra $P(f)$ at the receiver at the distance of 3 km from the source. Note that it is $P(f)$ that is usually required for assessing environmental impact of a given sound source as this quantity has to be multiplied by auditory frequency weighting functions of different marine animals. Also, note that good agreement in $P(f)$ usually implies that the respective signal waveforms agree well. By contrast, a good agreement of signal waveforms could possibly conceal discrepancies in the spectra, especially at the frequencies over which a relatively small portion of acoustic energy is distributed but which could become important after performing auditory frequency weighting.

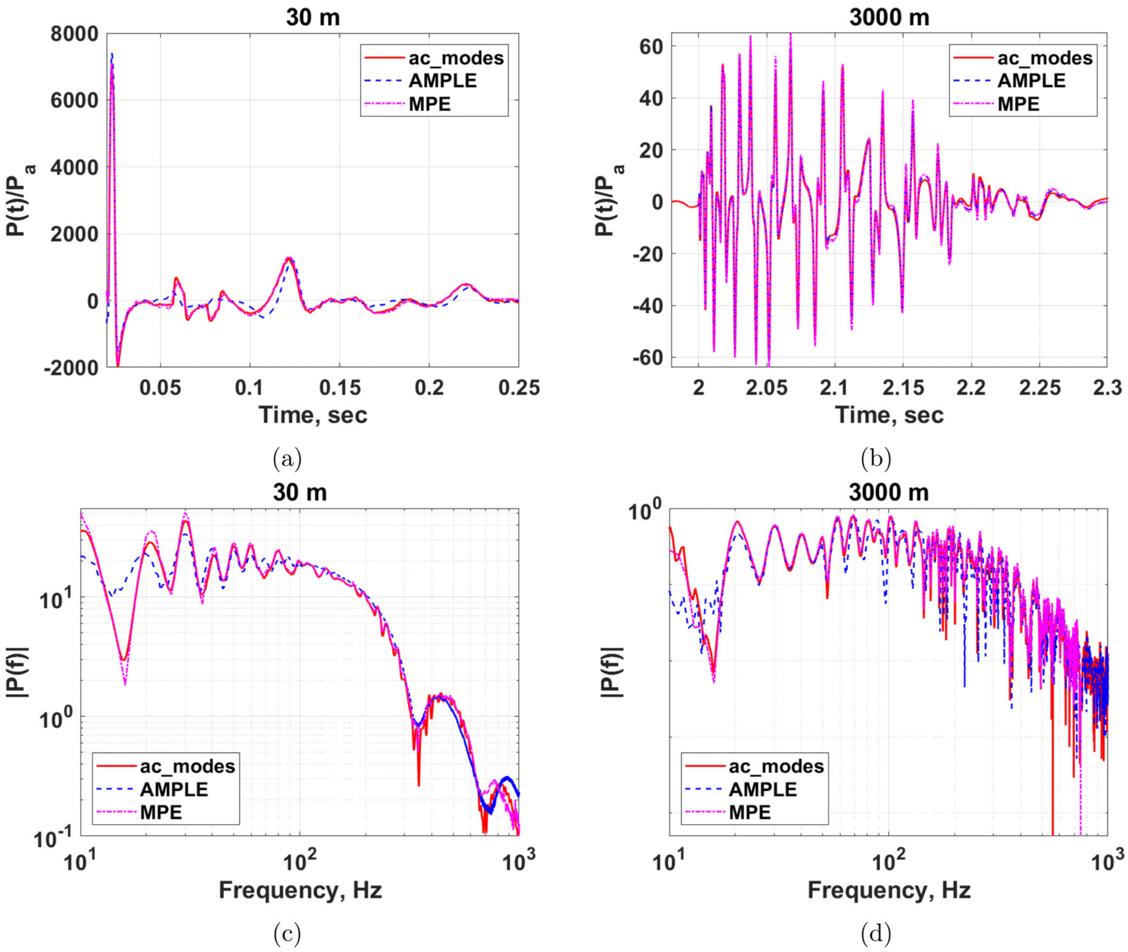

FIG. 6. (Color online) Acoustic pressure waveforms $p(t)$ for the environment depicted in Fig. 5(a) (range-independent case B1) at the receivers at ranges 30 m (a) and 3000 m (b) and their respective spectra $P(f)$ [(c), (d)] computed using `AMPLE` (dashed blue), `MPE` (solid red), and `ac_modes` (dashed-dotted magenta) are shown.

Assume that the source-receiver line (x axis) is aligned along the isobath [see Fig. 5(b)], i.e., that water depth $h(x,y)$ in the area is described by

$$h(x,y) = h_0 + \tan \alpha \cdot y,$$

where slope angle α assumes the values of 0.5°, 1°, and 1.5°, which are typical for continental shelf, and $h_0 = 50$ m, as in Secs. III and IV.

To validate our models in such a scenario, we compare the spectra with an analytical solution by the method of source images (Deane and Buckingham, 1993), which is considered to be a benchmark for the wedge problem. The computation results for all three slope angles are shown in Fig. 8. With logarithmic scaling of the frequency axis, it might appear that `AMPLE` and `MPE` solutions perfectly coincide with the analytical solution. However, a close-up in Fig. 8(d) reveals that for frequencies above 200 Hz, `MPE` exhibits certain inaccuracies (especially for the slope angle of1.5°), whereas `AMPLE` shows very good agreement with source images method up to 1 kHz. Inaccuracy of the `MPE` solution at certain high frequencies can be explained by somewhat unreliable behavior of the Crank-Nicholson-type numerical scheme, which is used for solving coupled MPEs. Note, however, that the comparison of received signals results in excellent agreement of all three methods (we do not show it here as, in our opinion, spectra in this case are more informative, whereas time-domain signal comparison conceals discrepancies at higher frequencies).

Despite noticeable differences between the spectra $P(f)$ for different slope angles, one can observe from Fig. 8 that, "on average," they demonstrate very similar behavior. This can be confirmed by comparing acoustic energy distribution at the receiver over decidecade frequency bands [it can be computed by integrating $|P(f)|^2$ with respect to the frequency over each band]. This distribution is shown in Fig. 10 for all three slope angle values and both source images solutions as well as the solution obtained by `AMPLE`. All six curves almost agree perfectly with each other.

We, therefore, have shown that although horizontal refraction in the wedge significantly changes the interference pattern of acoustic field, for relatively small distances of few kilometres from the source, it virtually does not affect integrals of acoustic energy over decidecade frequency bands that are usually used for the noise impact estimation. Partially, this result justifies the use of efficient

https://doi.org/10.1121/10.0034424

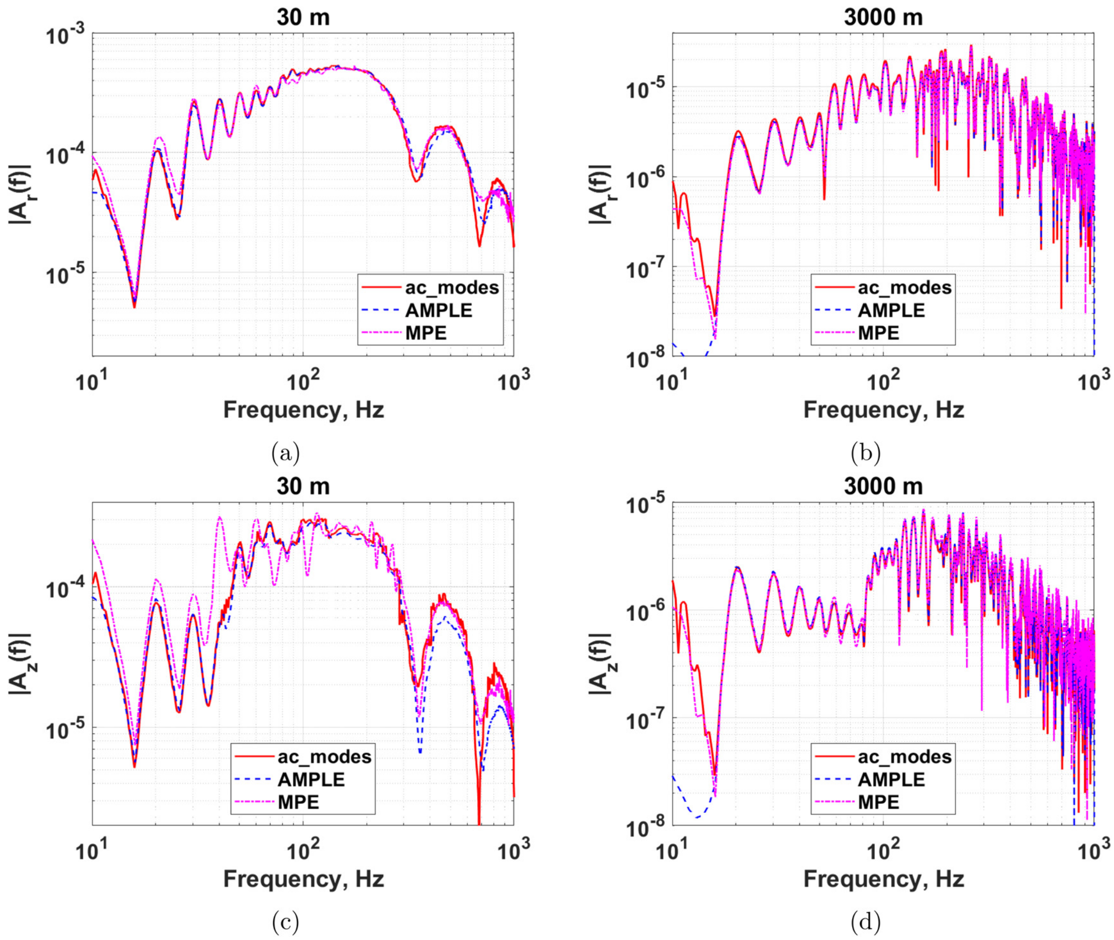

FIG. 7. (Color online) The spectra of the horizontal [(a), (b)] and vertical [(c), (d)] components (i.e., $|A_r(f)|$ and $|A_z(f)|$) of particle acceleration at the receivers at ranges 30 m and 3000 m are shown.

modern methods, such as SOPRANO (Sertlek *et al.*, 2019), that do not take 3D effects into account for noise estimation purposes.

VI. DOWNSLOPE PROPAGATION

In this section, we consider downslope broadband propagation, i.e., for the bathymetry described by the function

$$h(x, y) = h_0 + \tan\alpha \cdot (x - L/2),$$

where $\alpha = 0.5°$, $1°$, and $1.5°$, $L = 3$ km, and $h_0 = 50$ m (i.e., average water depth along the path of length L is exactly the same as in previous cases). In this section, we also assume that the receiver depth is 10 m (not 15 m as previously). Note that as a result of the reciprocity principle, $P(f)$ are exactly the same for positive and negative values of slope angle α, i.e., for upslope and downslope propagation. The respective comparison was performed as a consistency check for each model involved in this study (figures are not included here). Again, we restrict our attention to the computation of acoustic pressure spectra $P(f)$, as all other quantities (pulse waveform, particle accelerations, etc.) can be computed from it reliably and without any additional effort.

In Fig. 9, we present the simulation results for the downslope propagation case. As in Sec. V, they are validated by the comparison with the source images solution. As can be observed from Fig. 9, for the slope angle of 0.5°, MPE and AMPLE demonstrate perfect agreement with the reference solution [see Fig. 9(a)]. For $\alpha = 1°$ AMPLE is relatively accurate (modulo some small discrepancies) only for $f > 40$ Hz [Fig. 9(b)], while for $\alpha = 1.5°$, the agreement can be characterized as, at best, qualitative for the frequencies $f > 100$ Hz [Fig. 9(c)]. This result highlights the role of mode coupling, which is adequately taken into account by MPE model and completely neglected in AMPLE. Indeed, MPE perfectly agrees with the source images solution for low frequencies (i.e., for $f < 200$ Hz). Certain discrepancies and outliers at higher frequencies indicate that the respective numerical scheme becomes somewhat unreliable for $f >$ 300–400 Hz [see also close-up in Fig. 9(d)].

Thus, we can conclude that mode coupling is relatively insignificant for bottom slope angles below $\alpha < 1°$, and AMPLE can handle such problems accurately and efficiently. At the same time, when the path is aligned along the depth gradient and the slope angle $\alpha > 1°$, it is necessary to take the mode interaction into account, and the adiabatic horizontal refraction equations [Eq. (3)] are no longer adequate.

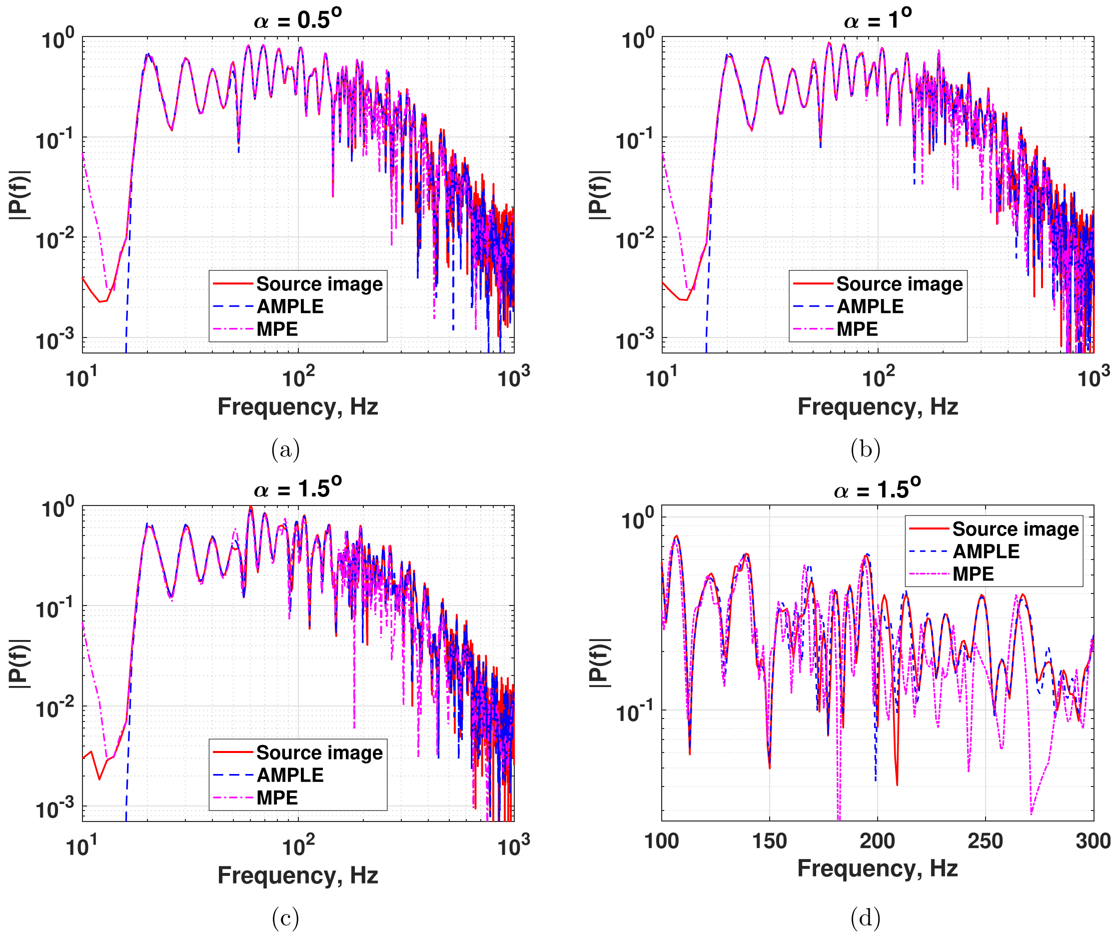

FIG. 8. (Color online) Acoustic pressure spectra $P(f)$ at $x = 3$ km, $y = 0$, $z = 15$ m computed using `AMPLE` (dashed blue), `source images` (Deane and Buckingham, 1993) (solid red), and `MPE` (dashed-dotted magenta) are shown for bottom slope angles *across the path* (a) $\alpha = 0.5°$, (b) $\alpha = 1°$, and (c) $\alpha = 1.5°$. (d) shows a close-up view of the case $\alpha = 1.5°$ at medium frequencies.

`MPE` is designed to deal with this effect, and it handles it very well for sufficiently low frequencies.

Let us now consider how the energy distribution over decidecade bands changes as the bottom slope along the path increases. The corresponding plots are shown in Fig. 10(b) for `AMPLE` and the reference solution by the source images. It is clear that, unlike in the case of across the slope propagation, water depth variations along the path (for the same fixed average value h_0) significantly increase transmission loss. It is also clear that for $\alpha = 0°$, `AMPLE` reproduces the distribution very accurately, whereas for larger slope angles, the agreement is reasonably good only for sufficiently high frequencies.

VII. CONCLUSION AND DISCUSSION

In this study, we discuss the solution of the test problems A1 and B1 that were proposed to the participants of the JAM Workshop 2022. Both of them are typical shallow-water sound propagation scenarios with the same geoacoustic parameters of the environment, and the key difference is that B1 deals with a broadband source. The problems were solved by the two models `MPE` and `AMPLE`, based on the MPEs theory developed at our laboratory at Pacific Oceanological Institute (Vladivostok, Russia) in the past 10 years. The configuration of both models is described, and the computational times required to handle both cases are reported. It is revealed that both models reliably reproduce the reference solutions for the original range-independent scenarios (during the workshop, the results were also verified against many other models used by other participants, and no major discrepancies were observed). We also study a modified B1 problem with the sloping bottom for the cases when depth gradient is aligned along and across the propagation path. In the former case, normal mode coupling comes into play for the slope angle $\alpha > 1°$, and the accuracy of `AMPLE` solution becomes insufficient for sound frequencies at which all or almost all waterborne modes encounter their cut-off depths at certain points of the path. In the case of propagation across the bottom slope, `AMPLE` confidently handles all tilt angles as in such scenarios, primary role is played by the horizontal refraction that is very accurately simulated by MPEs. On the other hand, `MPE` shows very accurate results for all bottom slope angles across and along the path for frequencies up to 250–300 Hz. For higher frequencies, standard (non-SSP) MPE marching scheme,

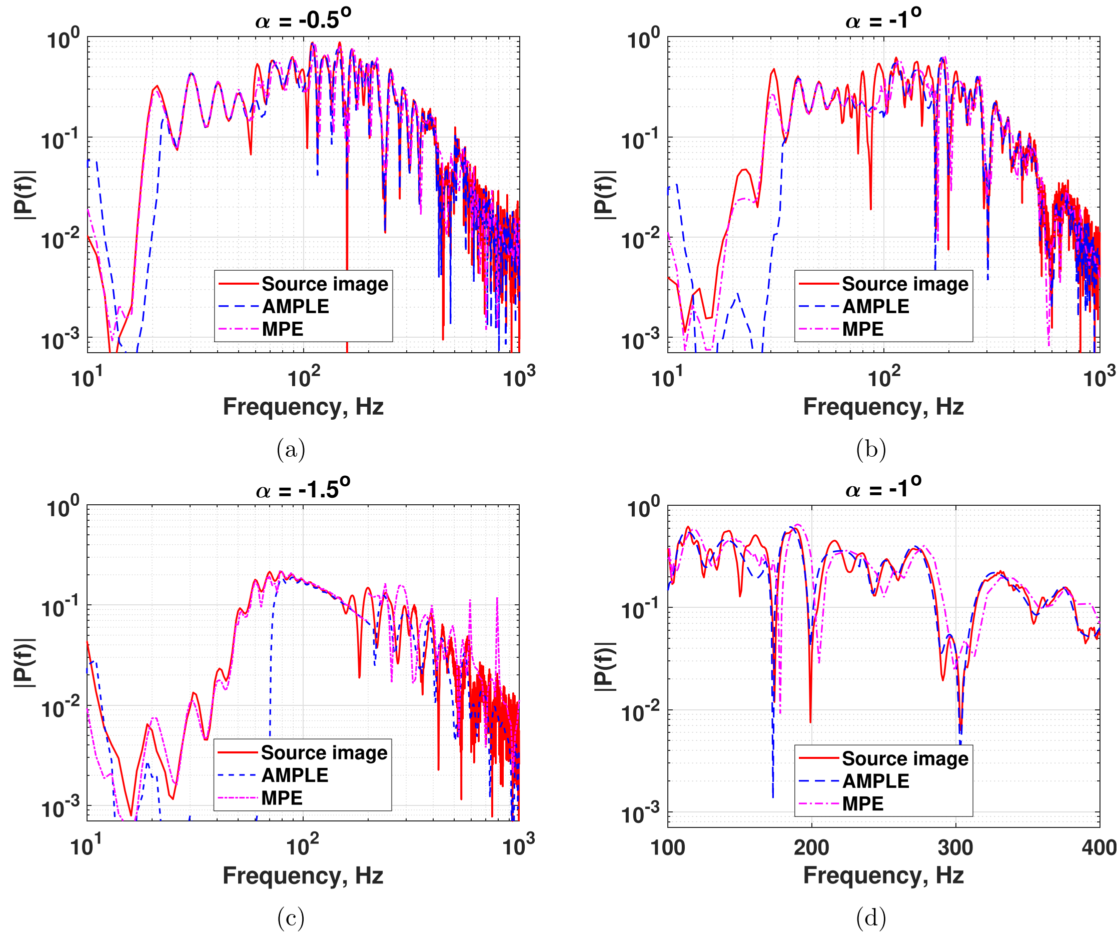

FIG. 9. (Color online) Acoustic pressure spectra $P(f)$ at $x = 3\,\mathrm{km}$, $y = 0$, $z = 10\,\mathrm{m}$ computed using AMPLE (dashed blue), source images (Deane and Buckingham, 1993) (solid red), and MPE (dashed-dotted magenta) are shown for bottom slope angles *along the path* (a) $\alpha = -0.5°$, (b) $\alpha = -1°$, and (c) $\alpha = -1.5°$. (d) shows a close-up view of the case $\alpha = -1°$ at medium frequencies.

however, requires step sizes that are too small for practice and, in general, becomes somewhat unreliable.

Obviously, the models based on the normal modes theory are particularly efficient for the scenarios in which the field can be accurately described by a few modes. For such cases, normal modes, in general, and MPE theory, in particular, work as model order reduction tools. This criterion is met in the cases involving frequencies from 50 to 500 Hz in

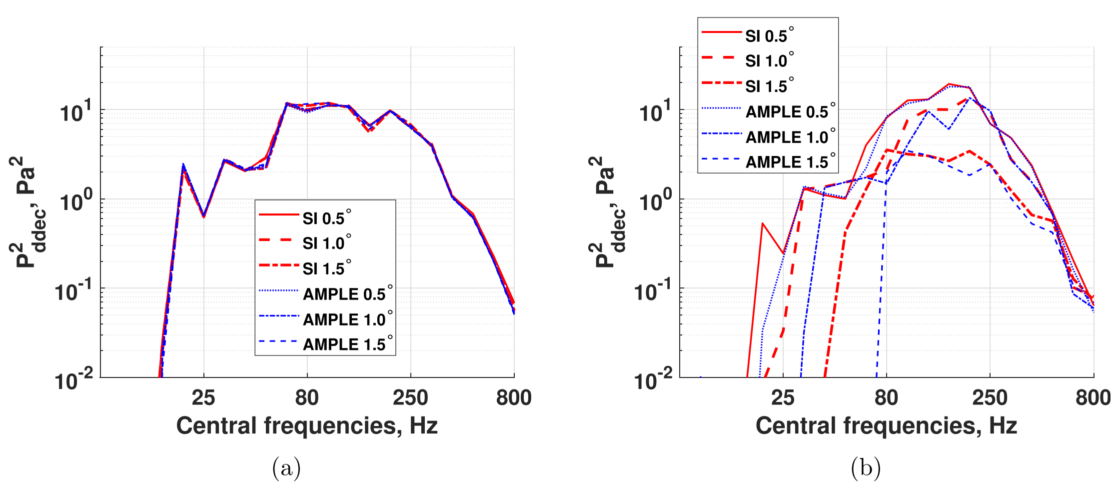

FIG. 10. (Color online) Signal energy distribution over decidecade frequency bands is shown for the cases of across-slope propagation (a) and downslope propagation (b).

case A1 and for the far-field receiver in case B1. Under these conditions, MPE-based models can significantly outperform computational tools based on 3D PEs (Petrov *et al.*, 2020; mainly because of quasi-separation of variables by normal mode expansion and the powerful SSP method). For complicated 3D environments, where it is hard to reliably identify all eigenrays connecting the source and the receiver, MPE could be expected to be more robust than the methods based on the ray theory and Gaussian beams. On the other hand, for a near-field receiver, virtually any other approach (including ray theory, traditional PEs, and wavenumber integration) would surely outperform MPEs. Our approach is also somewhat inefficient in the case of frequencies for which the waveguide admits no waterborne modes (e.g., for 10 Hz in the considered case). In such situations, the field can be accurately represented only by a relatively large number of "bottom" modes approximating branch line integral corresponding to continuous spectrum of the Pekeris waveguide (Jensen *et al.*, 2011).

It is important to stress that the efficiency and accuracy of the MPE-based models reported in this study will be retained in much more complicated 3D scenarios of sound propagation in shallow water. In particular, `MPE` and `AMPLE` can handle inhomogeneous bathymetry and sound speed profiles in the water column at almost no additional computational cost (Manul'chev *et al.*, 2022). Arguably, in many situations, it could also be important to take bottom elasticity into account when performing sound field modeling for the purposes of environment impact assessment. It can be performed with the framework of MPEs using the approach outlined in Kozitskiy (2022), although additional research efforts in this direction are required.

We also would like to emphasize the findings of this study on the relative importance of 3D effects (horizontal refraction) and mode coupling for noise simulation problems. Although the former could significantly change signal waveform and interference patterns of its time-harmonic components, at distances of few kilometres from the source, its effect fades away after the averaging over decidecade frequency bands (which is often performed for noise monitoring purposes). Therefore, for the distances similar to those in the B1 scenario, the use of 2D propagation models can be justified by this fact. On the other hand, for longer distances (e.g., 10 km), it has been previously shown that not only a full 3D model is required, but also it must have sufficient wide-angle capabilities to properly handle the effect of horizontal refraction (Manul'chev *et al.*, 2022). The simulation results presented above also indicate that adiabatic sound propagation models are adequate for shallow-water environments with typical bottom slope angles $\alpha < 1^\circ$ (within the frequency range from 10 Hz to 1 kHz). For greater angles, it is necessary to take mode interaction into account as well (otherwise, the results could be very inaccurate even after averaging over frequency bands). Although the current version of `AMPLE` does not have this capability, it can be implemented using a generalized SSP method proposed in Petrov *et al.* (2024).

ACKNOWLEDGMENTS

The authors are grateful to Vladimir Nechayuk and Michael Jenkerson (Exxon Mobil) for inviting P.S.P. to participate in the workshop as well as for their useful comments. We also thank Dr. Michael Porter (HLS Research) for making his simulation results available for comparison. We are also immensely grateful to Dr. Michael Ainslie and the JASCO team who organized the workshop and provided us with all of the help and guidance that we needed. The work of M.A.S., A.G.T., and S.B.K. was supported by the Russian Science Foundation, Project No. 22-11-00171, which is available online.[2]

AUTHOR DECLARATIONS

Conflict of Interest

The authors have no conflicts to disclose.

DATA AVAILABILITY

Data sharing is not applicable to this article as no new data were created or analyzed in this study.

[1]See https://github.com/kaustikos/ac_modes (Last viewed 24 October 2024).
[2]See https://rscf.ru/en/project/22-11-00171/ (Last viewed 24 October 2024).

Abawi, A., Kuperman, W., and Collins, M. (**1997**). "The coupled mode parabolic equation," J. Acoust. Soc. Am. **102**(1), 233–238.

Abawi, A. T. (**2002**). "An energy-conserving one-way coupled mode propagation model," J. Acoust. Soc. Am. **111**(1), 160–167.

Ainslie, M., Heaney, K., and MacGillivray, A. (**2019a**). "Guest editorial special issue on verification and validation of air gun source signature and sound propagation models," IEEE J. Ocean. Eng. **44**(3), 551–559.

Ainslie, M. A., Halvorsen, M. B., and Robinson, S. P. (**2022**). "A terminology standard for underwater acoustics and the benefits of international standardization," IEEE J. Ocean. Eng. **47**(1), 179–200.

Ainslie, M. A., Laws, R. M., and Sertlek, H. Ö. (**2019b**). "International airgun modeling workshop: Validation of source signature and sound propagation models—Dublin (Ireland), July 16, 2016—Problem description," IEEE J. Ocean. Eng. **44**(3), 565–574.

Ainslie, M. A., Laws, R. M., Smith, M. J., and MacGillivray, A. O. (**2024**). "Source and propagation modelling scenarios for environmental impact assessment: Verification," J. Acoust. Soc. Am. **156**, 1489–1508.

Collins, M. D. (**1993**). "The adiabatic mode parabolic equation," J. Acoust. Soc. Am. **94**(4), 2269–2278.

Deane, G., and Buckingham, M. (**1993**). "An analysis of the three-dimensional sound field in a penetrable wedge with a stratified fluid or elastic basement," J. Acoust. Soc. Am. **93**(3), 1319–1328.

Godin, O. A. (**1998**). "A note on differential equations of coupled-mode propagation in fluids," J. Acoust. Soc. Am. **103**(1), 159–168.

ISO (**2017**). 18405:2017, "Underwater acoustics—Terminology" (International Organization for Standardization, Geneva, Switzerland).

Jensen, F. B., Kuperman, W. A., Porter, M. B., and Schmidt, H. (**2011**). *Computational Ocean Acoustics* (Springer Science and Business Media, New York).

Katsnelson, B., Petnikov, V., and Lynch, J. (**2012**). *Fundamentals of Shallow Water Acoustics* (Springer Science and Business Media, New York).

Kozitskiy, S. (**2022**). "Coupled-mode parabolic equations for the modeling of sound propagation in a shallow-water waveguide with weak elastic bottom," J. Mar. Sci. Eng. **10**(10), 1355.

Manul'chev, D., Tyshchenko, A., Fershalov, M., and Petrov, P. (**2022**). "Estimating sound exposure levels due to a broadband source over large areas of shallow sea," J. Mar. Sci. Eng. **10**(1), 82.

Petrov, P., and Tyshchenko, A. (**2020**). "Ample mode parabolic equation," available at https://github.com/GoldFeniks/Ample (Last viewed 24 October 2024).

Petrov, P., Zaikin, O., and Tyshchenko, A. (**2019**). “Cambala: Coupled acoustic modes with bottom attenuation in linear acoustics,” available at https://github.com/Nauchnik/CAMBALA (Last viewed 24 October 2024).

Petrov, P. S., and Antoine, X. (**2020**). “Pseudodifferential adiabatic mode parabolic equations in curvilinear coordinates and their numerical solution,” J. Comput. Phys. **410**, 109392.

Petrov, P. S., Ehrhardt, M., and Kozitskiy, S. B. (**2024**). “A generalization of the split-step Padé method to the case of coupled acoustic modes equation in a 3D waveguide,” J. Sound Vib. **577**, 118304.

Petrov, P. S., Ehrhardt, M., Tyshchenko, A. G., and Petrov, P. N. (**2020**). “Wide-angle mode parabolic equations for the modelling of horizontal refraction in underwater acoustics and their numerical solution on unbounded domains,” J. Sound Vib. **484**, 115526.

Petrov, P. S., and Sturm, F. (**2016**). “An explicit analytical solution for sound propagation in a three-dimensional penetrable wedge with small apex angle,” J. Acoust. Soc. Am. **139**(3), 1343–1352.

Rutenko, A., Kozitskii, S., and Manul’chev, D. (**2015**). “Effect of a sloping bottom on sound propagation,” Acoust. Phys. **61**(1), 72–84.

Rutenko, A. N., Zykov, M. M., Gritsenko, V. A., Fershalov, M. Yu., Jenkerson, M. R., Manulchev, D. S., Racca, R., and Nechayuk, V. E. (**2022**). “Acoustic monitoring and analyses of air gun, pile driving, vessel, and ambient sounds during the 2015 seismic surveys on the Sakhalin shelf,” Environ. Monit. Assess. **194**(Suppl 1), 744.

Sertlek, H. Ö., Ainslie, M. A., and Heaney, K. D. (**2019**). “Analytical and numerical propagation loss predictions for gradually range-dependent isospeed waveguides,” IEEE J. Ocean. Eng. **44**(4), 1240–1252.

Trofimov, M., Kozitskiy, S., Zakharenko, A., and Petrov, P. (**2023**). “Formal derivations of mode coupling equations in underwater acoustics: How the method of multiple scales results in an expansion over eigenfunctions and the vectorized WKBJ solution for the amplitudes,” J. Mar. Sci. Eng. **11**(4), 797.

Trofimov, M. Y. (**1999**). “Narrow-angle parabolic equations of adiabatic single-mode propagation in a horizontally inhomogeneous shallow sea,” Acoust. Phys. **45**, 575–580.

Trofimov, M. Y., Kozitskiy, S., and Zakharenko, A. (**2015**). “A mode parabolic equation method in the case of the resonant mode interaction,” Wave Motion **58**, 42–52.

Trofimov, M. Y., Kozitskiy, S., and Zakharenko, A. (**2018**). “Simulation of the pulse propagation by the interacting mode parabolic equation method,” Comput. Phys. Commun. **228**, 54–60.

Tromp, J. (**1994**). “A coupled local-mode analysis of surface-wave propagation in a laterally heterogeneous waveguide,” Geophys. J. Int. **117**(1), 153–161.

Tyshchenko, A., Zaikin, O., Sorokin, M., and Petrov, P. (**2021**). “A program based on the wide-angle mode parabolic equations method for computing acoustic fields in shallow water,” Acoust. Phys. **67**, 512–519.